

Creation of Ghost Illusions Using Wave Dynamics in Metamaterials

Wei Xiang Jiang, Cheng-Wei Qiu,* Tiancheng Han, Shuang Zhang,
and Tie Jun Cui*

The creation of wave-dynamic illusion functionality is of great interest to various scientific communities because it can potentially transform an actual perception into the pre-controlled perception, thus empowering unprecedented applications in the advanced-material science, camouflage, cloaking, optical and/or microwave cognition, and defense security. By using the space transformation theory and engineering capability of metamaterials, a functional “ghost” illusion device, which is capable of creating multiple virtual ghost images of the original object’s position under the illumination of electromagnetic waves, is proposed and realized. The scattering signature of the object is thus ghosted and perceived as multiple ghost targets with different geometries and compositions. The ghost-illusion material, which is being inhomogeneous and anisotropic, is realized using thousands of varying unit cells working at non-resonance. The experimental demonstration of the ghost illusion validates the theory of scattering metamorphosis and opens a novel avenue to the wave-dynamic illusion, cognitive deception, manipulate strange light (or matter) behaviors, and design novel optical and microwave devices.

and the second is to create the desired scattering signature by employing additional spatial transformations. However, a number of implications are entailed by involving lossless double-negative metamaterial in the transformation.^[23–29] For instance, from theoretical point of view, not all objects have their complementary counterparts (e.g., perfect electric and magnetic conductors, gyrotropic objects, and chiral objects). In the mean time, it is too stringent in practice, if not impossible, to achieve lossless double-negative materials in electromagnetic and optical spectra. Hence, the loss will dramatically deteriorate the illusionary performance. In this connection, an improved illusion device consisting of only positive materials has been studied.^[16] However, extreme values of optical parameter are required, which would necessarily involve resonance effect that leads to narrow band operation,

1. Introduction

Transformation optics, a new designing tool based on space transformation, has enabled a number of unconventional optical devices, including perfect invisibility cloaks,^[1–7] carpet cloaks,^[8–14] illusion-optics devices,^[15–19] Eaton lens,^[20] and flattened Luneburg lenses.^[21,22] In particular, the creation of optical illusion has been of great interest since it may lead to many unprecedented applications.^[15–19] Illusion optics was proposed based on a two-fold operation.^[15] The first is to eliminate the scattering of the original object by using double-negative metamaterial,

not to mention the complexity of metamaterial designs.

Double-negative metamaterials may be easily obtained in composite transmission-line resistor-inductor-capacitor (RLC) circuits.^[17] Though the planar RLC circuits can exhibit the superscattering effect via the manipulations of voltage and impedance, it is inherently restricted to lumped circuitry on a circuit board, and thus cannot be considered as illusion per se, based on the light-matter interaction in free space governed by Maxwell’s equations. Beyond the circuit representation, two spatial wave-dynamic experiments have been demonstrated to manifest the real radar illusions.^[18,19] However, such experiments have critical restrictions: they can only simply reduce the size or change the material property of the original object, but cannot alter and shift the scattering center of the original object. That is to say, there is only a single illusion object located at the original position. Therefore, the observer can still perceive that there is one scattering center at the position of the object, though with different scattering signatures.

In this paper, we report a distinguished anisotropic-graded-material (AGM) based functional illusion device in the wave dynamics, which virtually transforms the scattering signature of an arbitrary object to that of multiple isolated ghost objects (i.e., not existing physically). In other words, the ghost illusion device can make the scattering signature of the “cloaked” object equivalent to that of multiple other objects, in both the near-field pattern and far-field scattering cross section, in which the

Dr. W. X. Jiang, Prof. T. J. Cui
State Key Laboratory of Millimeter Waves
Department of Radio Engineering
Southeast University
Nanjing 21009, China
E-mail: tjcu@seu.edu.cn

Prof. C.-W. Qiu, T. Han
Department of Electrical and Computer Engineering
National University of Singapore
119620, Singapore
E-mail: chengwei.qiu@nus.edu.sg

Prof. S. Zhang
School of Physics and Astronomy
University of Birmingham
Edgbaston, Birmingham, B15 2TT, UK



DOI: 10.1002/adfm.201203806

multiple ghost objects can be arbitrarily pre-designed and pre-controlled.

2. Functional Ghost Illusion Device

2.1. Concept and Analytical Design

The functions of the ghost illusion device are schematically illustrated in **Figure 1**, which transforms a perfectly conducting (or metallic) object in **Figure 1a** into three objects, including a shrunk metallic object in the original position and two “virtual” dielectric objects (which can also be metallic) on each side, as in **Figure 1c**. In comparison, the radar signature of the original metallic object is given in **Figure 1d**, showing the typical feature of a single target. When the metallic object is covered by the designed ghost illusion device (see **Figure 1b**), the corresponding radar signature is demonstrated in **Figure 1e**, which is completely different from **Figure 1d**, but exactly the same as that of three virtual objects (**Figure 1c**) shown in **Figure 1f**. Hence the ghost device shrinks the original metallic object and produces two additional ghost images in the radar signature. In other words, radar only perceives that there are three standalone objects, though only a single object (the real object with the ghost coating) is physically present at the center.

The above functionality can be directly derived using the transformation optics theory.^[2] In the actual space, the radius of the object (or the inner radius of the ghost device) is a , and the outer radius of the ghost device is c . In the virtual space, there are three distinct objects: a shrunk object and two wing-ghosts, as shown in **Figure 1c**. Here, we just design two wing-ghosts as an example. Actually, we can design arbitrary number of virtual objects, so that it is more rotationally symmetric and is less independent of the incident wave. The radius of shrunk object is a' and the inner and outer radii of wing-ghosts are b' and c . The general 3D optical transformation for the above functionality is written in the spherical coordinates as

$$(r, \theta, \varphi) = (k(r' - a') + a, \theta', \varphi') \quad (1)$$

in which $k = \frac{c-a}{c-a'}$. Then the constitutive parameters in the region from $r = a$ to $r = c$ except the two wing-ghost areas (see region I in **Figure 2c**) and the two wing-ghost areas (region II in **Figure 2c**) in the spherical coordinates can be obtained as

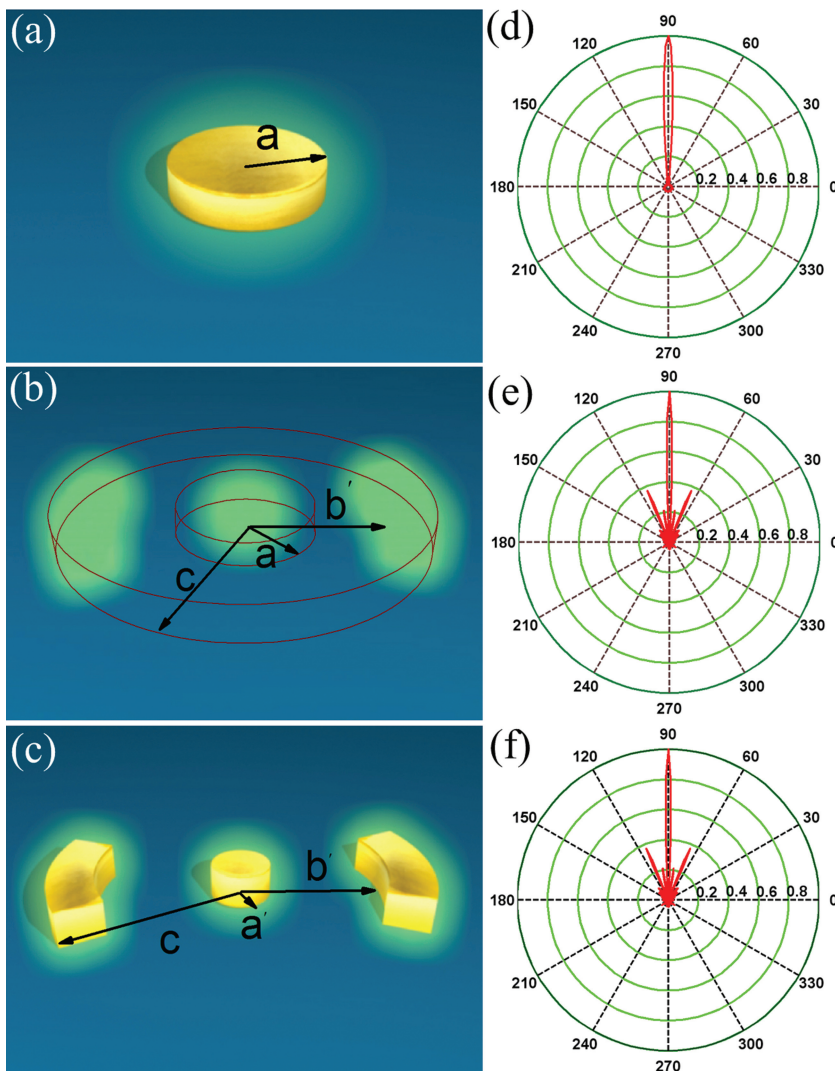


Figure 1. Schematic, composition, and equivalence of the ghost-illusion device. a) The original metallic object with its scattering signature given in panel (d) showing the typical feature of a single target. b) The metallic object covered by the designed ghost device whose physical boundaries are denoted with red solid lines and scattering signature is given in panel (e), metamorphosing scattering feature of the original object. c) A shrunk metallic object at the original center with two wing dielectric objects, whose signature is given in panel (f), showing the typical scattering feature of three objects. The scattering signatures of (b,c) are completely the same. In the far-field calculation, the geometrical parameters are chosen as $a = 3.8\lambda_0$, $a' = 1.63\lambda_0$, $b' = 5.4\lambda_0$ and $c = 7\lambda_0$.

$$(\varepsilon_r, \varepsilon_\theta, \varepsilon_\varphi) = (\mu_r, \mu_\theta, \mu_\varphi) = \left(\frac{1}{k} \left(\frac{r - a + ka'}{r} \right)^2, \frac{1}{k}, \frac{1}{k} \right) \quad (2a)$$

$$(\varepsilon_r, \varepsilon_\theta, \varepsilon_\varphi) = (\mu_r, \mu_\theta, \mu_\varphi) = \left(\frac{1}{k} \left(\frac{r - a + ka'}{r} \right)^2, \frac{1}{k}, \frac{\varepsilon_{\text{virtual}}}{k} \right) \quad (2b)$$

where, $(\varepsilon_r, \varepsilon_\theta, \varepsilon_\varphi)$ and $(\mu_r, \mu_\theta, \mu_\varphi)$ are the relative permittivity and permeability tensors, and $\varepsilon_{\text{virtual}}$ is the relative permittivity of the ghost-wing targets, which is a pre-designed and known parameter. Equation (2) describes the electromagnetic properties of a 3D ghost-illusion device. For the 2D case, the cross section

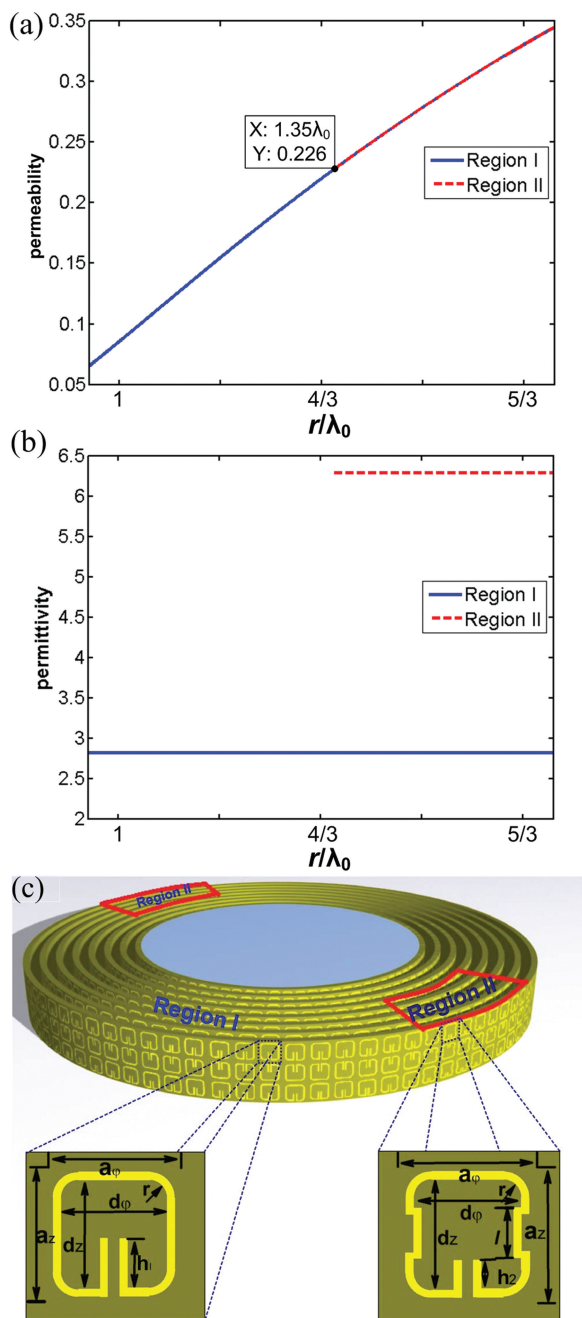


Figure 2. The design and fabrication of the simplified ghost device. a) The radial permeability in regions I and II as a function of radial variable r . b) The z -direction permittivity in regions I and II. c) The conventional and modified SRRs constitute the ghost device following the parameters described in Equation (2).

of the cylindrical ghost device is the same as in Figure 1. The cylindrical device is characterized by its diagonal-parameter tensors in the cylindrical coordinates (r, ϕ, z) , and the same equations shown above hold for the diagonal-components $(\mu_r, \mu_\phi, \mu_z, \epsilon_r, \epsilon_\phi, \epsilon_z)$ of full parameters. In order to be realized by artificial materials, the full parameter can be simplified under the

transverse-electric (TE) polarization. The simplified parameters of the 2D ghost-illusion device for z -polarized electric fields are written as

$$(\mu_r, \mu_\phi, \epsilon_z) = \left(\left(\frac{r - a + ka'}{r} \right)^2, 1, \frac{1}{k^2} \right) \quad (3a)$$

$$(\mu_r, \mu_\phi, \epsilon_z) = \left(\left(\frac{r - a + ka'}{r} \right)^2, 1, \frac{\epsilon_{\text{virtual}}}{k^2} \right) \quad (3b)$$

We illustrate the above medium parameters of the ghost device in regions I and II in Figure 2a,b as a function of radian variable r , in which the geometrical parameters are set by $a' = 0.41\lambda_0$, $a = 0.95\lambda_0$, $b' = 1.08\lambda_0$, $c = 1.75\lambda_0$, $\epsilon_{\text{virtual}} = 2.23$, and the free-space wavelength $\lambda_0 = 30\text{ mm}$ at the frequency of 10 GHz. From Figure 2a,b, we notice that the relative permittivity in two regions are 2.82 and 6.29, respectively, and the relative permeability ranges from 0.06 to 0.35, which can be realized by using artificial materials.

2.2. Material Synthesis and Device Fabrication

In region I, the permittivity maintains 2.82 and the permeability ranges from 0.065 to 0.226, which are realized by artificially structured materials—the conventional split-ring resonators (SRRs) etched on a dielectric substrate; while in region II, the permittivity maintains 6.29 and the permeability ranges from 0.226 to 0.355, which are realized by a class of modified SRRs shown in Figure 2c. Such modified SRR structures can raise the permeability remarkably. In our design, there are two methods to generate the required high electric permittivity (6.29) in Region II without using any auxiliary high-permittivity materials. One is to add some curved structures to SRRs, and the other is to reduce the wire width of SRRs.

The designed ghost device illustrated in Figure 2c is synthesized with eight concentric layers of low-loss printed circuit boards (PCBs). On each layer, SRRs of 35 μm -thick copper was coated on one side of the 0.25 mm-thick substrate (F4B) with the relative permittivity $\epsilon = 2.65 + i0.003$. Although we apply different structures in Regions I and II, the height of each layer ($0.36\lambda_0$, 10.8 mm) and the distance between adjacent layers ($\lambda_0/10$, 3 mm) remain the same. The inner and outer radii of the ghost device are $0.95\lambda_0$ and $1.75\lambda_0$, respectively. Each layer carries three rows of SRRs, whose length and height are 3.14 mm and 3.6 mm. The designed SRRs create the required radial permeability μ_r and z -direction permittivity ϵ_z at 10 GHz. The PCB rings are adhered to a 2-mm-thick hard-foam board that was cut with concentric circular rabbets to fit the concentric layers exactly.

2.3. Full-Wave Simulation Results

The performance of the ghost device is numerically verified at the operating frequency of 10 GHz ($\lambda_0 = 30\text{ mm}$), in which the geometrical parameters are chosen to be the same as those in later experiments: $a' = 0.41\lambda_0$, $a = 0.95\lambda_0$, $b' = 1.08\lambda_0$, $c = 1.75\lambda_0$,

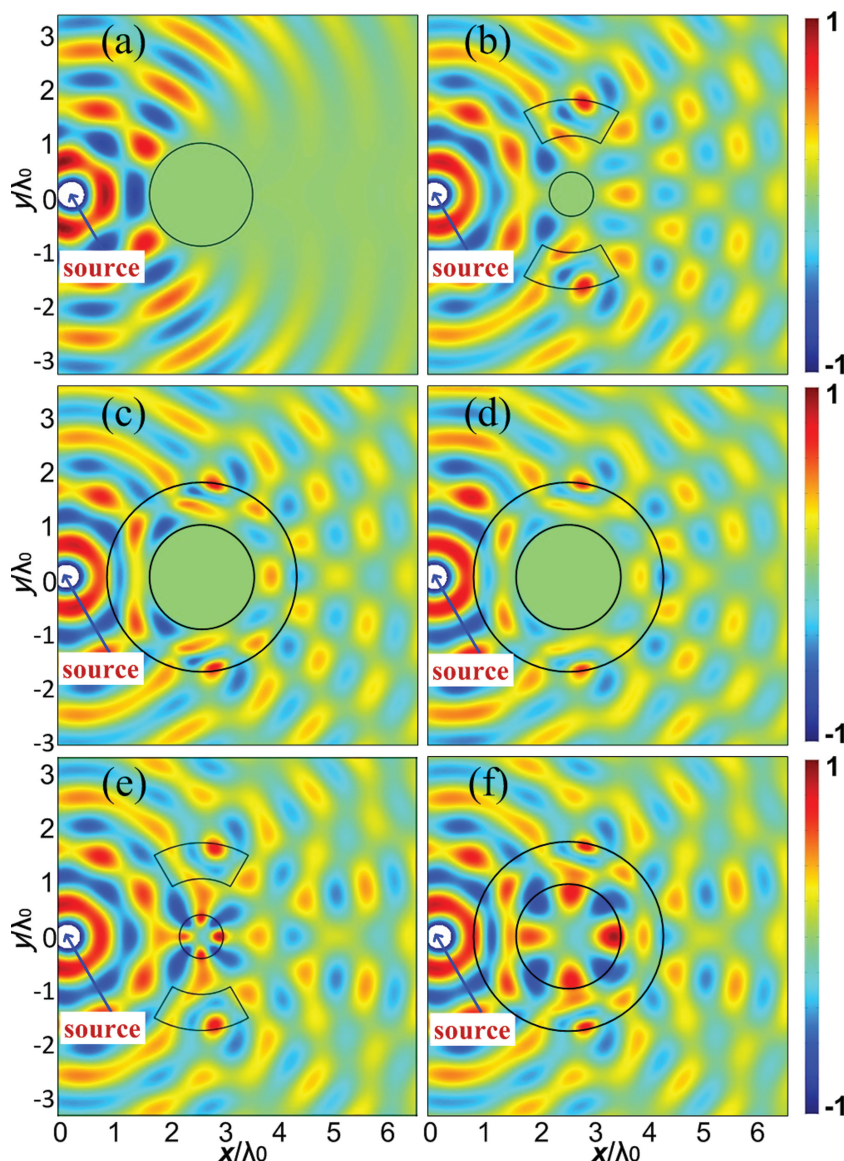


Figure 3. Full-wave simulation results of electric-field distributions for different cases. a) A bare metallic cylinder, whose scattering signature has a big shadow in the forward direction. b) The virtual objects: a smaller metallic cylinder in the center with two dielectric wing objects, whose scattering signature is completely metamorphosed. c) The metallic cylinder wrapped by full-parameter ghost device, whose signature is identical to that of three virtual objects. d) The metallic cylinder wrapped by the reduced-parameter ghost device, whose scattering signature is nearly the same as that of three virtual objects. e) The virtual objects: a smaller dielectric cylinder in the center with two dielectric wing objects. f) The dielectric cylinder wrapped by the full-parameter ghost device, whose signature is identical to that of three virtual objects.

and $\varepsilon_{\text{virtual}} = 2.23$. The distance between the source and the center of ghost device is $2.43\lambda_0$. The numerical simulation results are presented in **Figure 3**, in which (a) and (c) illustrate the electric-field distributions of a metallic cylinder without and with the full-parameter ghost device, respectively, under the excitation of a line source.

Figure 3b shows the electric fields of a small metallic cylinder with two standalone dielectric wings, which are characterized by the relative permittivity 2.23. The effectiveness of the ghost device in creating radar ghost images is confirmed

via the equivalence between the identical patterns in Figure 3b,c outside the outermost boundary. In other words, the proposed ghost device virtually camouflages the initial radar image of a metallic cylinder by illusion radar images of three objects. More interestingly, two ghost images appear separately apart from the original position, which totally change the signature of the given target. In order to facilitate the fabrication in experiments, it is necessary to consider and check the performance of the simplified ghost device, whose electric-field patterns are illustrated in Figure 3d. It can be seen that the radar signature of the metallic cylinder coated with the simplified ghost device is nearly the same as those in Figure 3b,c. Hence it is justified to use the simplified parameters as the experimental verification of the ghost effects.

The ghost device is also effective for dielectric objects. For example, we can simply choose the object as free space (or air) with the same geometrical parameters. The numerical simulation results are demonstrated in Figure 3e,f, from which we observe that such a ghost device can virtually transform the void (i.e., air) into the electromagnetic images of three distinct objects. It is noted that the ghost device not only shrinks the central air area, but also changes the material properties virtually.

2.4. Experimental Results

Figure 4a illustrates the experimental setup together with the resultant 2D fields in the near zone. The electric field depends on x and y coordinates, but does not vary in the z direction, which is the direction of polarization parallel to the antenna's orientation. In the experiment, the distance between the source and the center of ghost device is set as $3.93\lambda_0$. **Figure 4b–d** show the simulation and measurement results of the ghost device. As illustrated in **Figure 4b**, the measured electric fields inside the ghost device are perturbed by AGM, but the scattered waves outside are in very good agreement to the numerical results for a layered ghost-device profile, as shown in **Figure 4d**. For more details, **Figure 4c** compares the simulated and measured electric field intensity along a pre-selected line, located at $3.8\lambda_0$ (114 mm) away from the ghost device. In this experiment, the ghost device has just 8 layers including two regions as **Figure 2b** shows, and we are already able to observe good illusion performance. The simplified prototype preserves the functionality of the ideal ghost device, indicating the robustness of the design for practical applications.

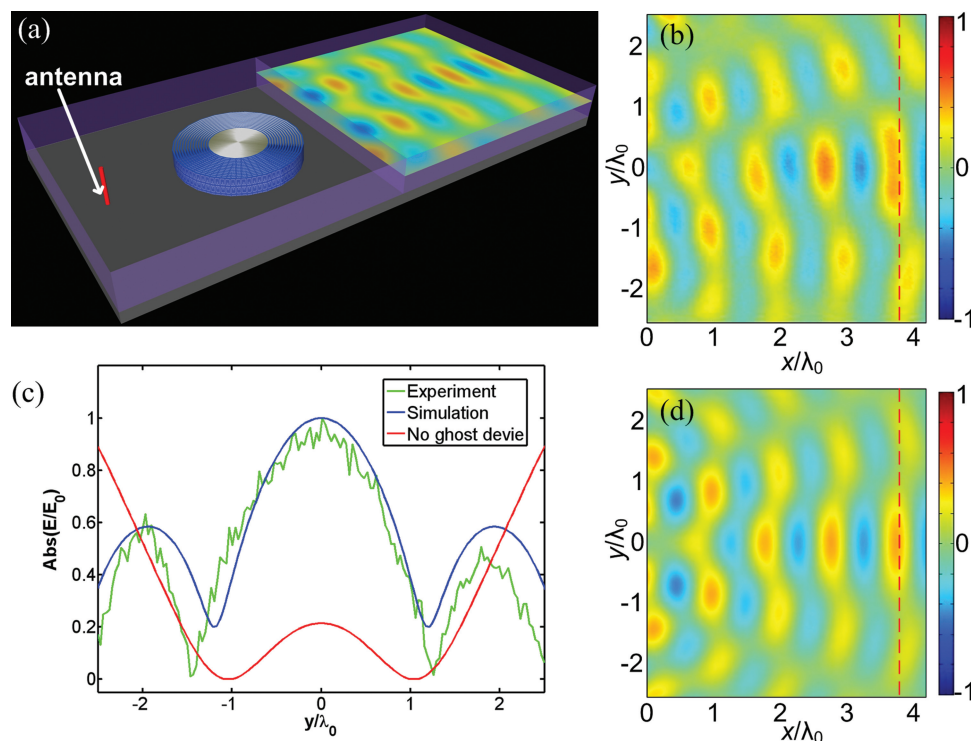


Figure 4. The experimental setup, simulation and experimental results of the ghost-illusion device. a) Illustration of the experimental setup. b) The measurement result. c) The normalized intensity along the red dashed line $x = 3.8\lambda_0$. d) The simulation result. The simulation and experiment results have good agreements, demonstrating the ghosting phenomena in scattering signatures.

3. Extending Functionalities

In the above simulation and experiment results, we have discussed and validated one situation of the ghost device, which transforms a metallic object in the real space into a smaller metallic object with two standalone dielectric wings in the virtual space. It is noted more types of ghost scattering can be produced under other design configurations. For example, when we choose $a' = 0$ mm (i.e., the radius of metallic cylinder is zero in the virtual space) with other parameters unchanged, then the device will produce only two ghost-wing objects. The full-wave simulation results of electric fields are presented in Figure 5a,b, in which (a) indicates the scattering pattern of two standalone dielectric wings with relative permittivity 2.23, and (b) illustrates the electric-field distribution of a copper cylinder covered by the ghost device. The effectiveness of the ghost device in creating the illusion is obviously pronounced via the identical patterns in these two subfigures outside the outer boundary. In other words, this ghost device virtually camouflages the initial electromagnetic scattering of a metallic cylinder, as if there were only those of two dielectric objects. It is very important that there will be no scattering center in the original position of the actual target in this case.

When the two wings of ghost device are metallic, they are also effective for the dielectric and metallic objects. Figure 5c–f illustrate two cases of ghost devices with metallic wings. In Figure 5c,d, the ghost device shrinks a copper cylinder to nothing but virtually produces two wing metallic objects; in Figure 5e,f, the shrunk object is dielectric while the

two wings are metallic. In both cases, the excellent ghost-illusion performance is clearly observed.

Furthermore, if we divide region II into several smaller areas or consider more blocks of region II, the ghost device will transform the signature of one object to an equivalence of a cluster of multiple different objects. Hence, many interesting illusion performance can be manipulated via the proposed ghost devices. Introducing more blocks of region II can also make the device rotationally symmetric, thus becoming more independent of the incident direction.

4. Conclusions

We have conjectured, fabricated, and demonstrated a general ghost-illusion device enabling an object to possess arbitrary wing-ghosts off its original position and produce virtual images. The principle can be precisely controlled for producing the desired scattering metrics of the ghost device. Metamaterial structures using thousands of SRRs are employed to realize the 2D prototype, so that the ghost signatures are produced at non-resonant frequency with low-loss feature thereby. The metamorphosis of electromagnetic signature has been verified by numerical investigation and experiments, which demonstrate good ghost-illusion performance in wave dynamics. Such a method is scalable in different frequency regions, provided that the future nanofabrication technique can produce the required subwavelength elements in the infrared or visible light.

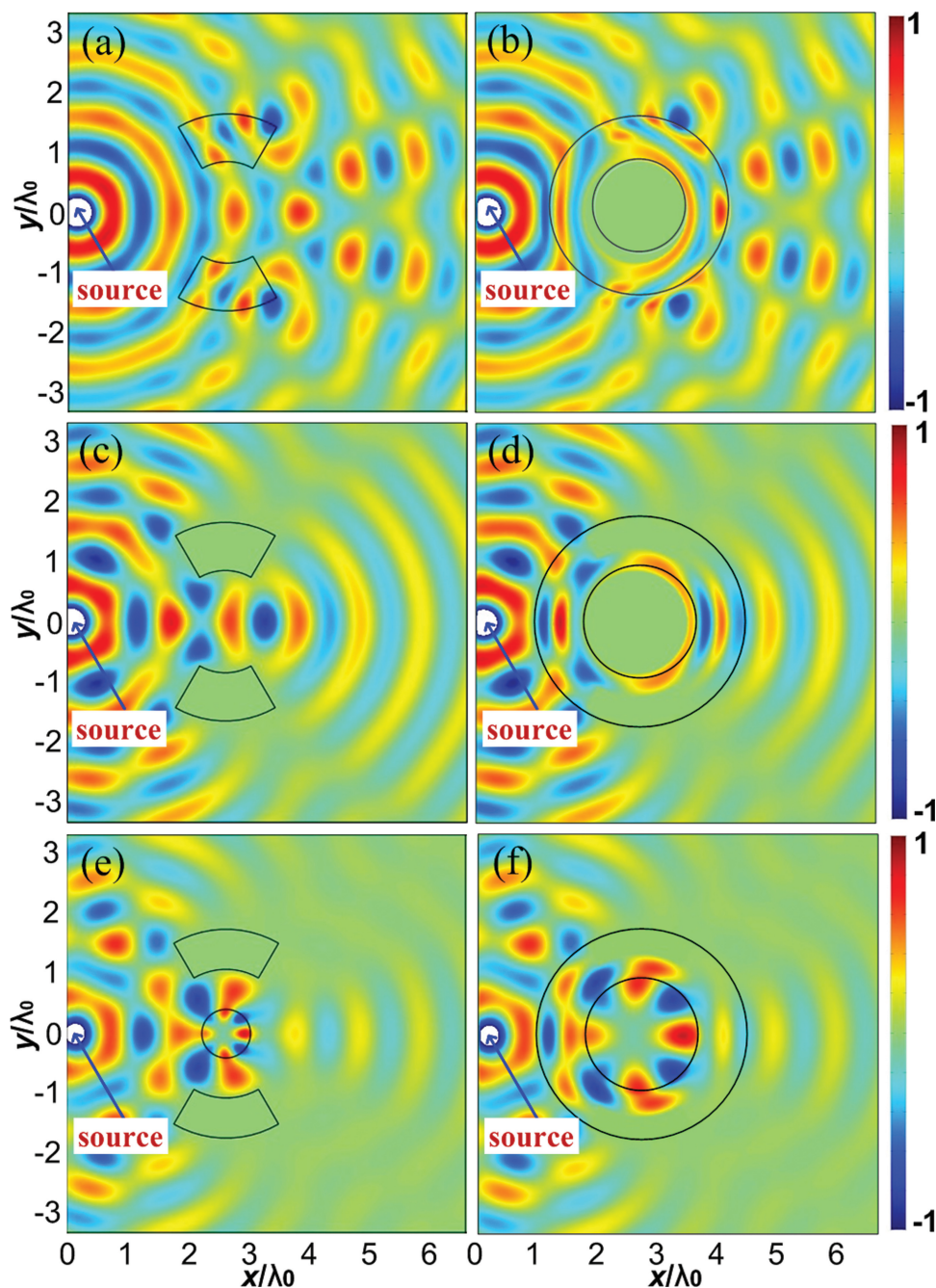


Figure 5. Simulation results of other functional ghost-illusion devices. a,b) A ghost device shrinks a metallic cylinder to nothing and virtually produces two wing dielectric objects. c,d) A ghost device shrinks a metallic cylinder to nothing and virtually produces two wing metallic objects. e,f) A ghost device shrinks a dielectric object and virtually produces two wing metallic objects.

In contrast to cloaking, the ghost devices empowers a novel way to alter the scattering signatures of targets to be “ghosted”. The observer cannot distinguish, and the readout can thus be misled. The object is there, but you do not see it while you see “them” elsewhere instead. More importantly, the proposed approach can deal with arbitrary target (e.g., perfectly electrical conductor) in wave dynamics without negative-index complementary media,^[23–29] and the ghost is pre-controllable. The current work may provide unprecedented avenue to the

light-matter behavior control and security enhancement, which advances beyond the earlier illusion devices.^[15–19]

5. Experimental Section

Experimental Setup and Field Mapping: A vector network analyzer (Agilent PNA-LN5230C) was used to excite and receive the microwave signals and a parallel-plate mapping system was applied to scan the

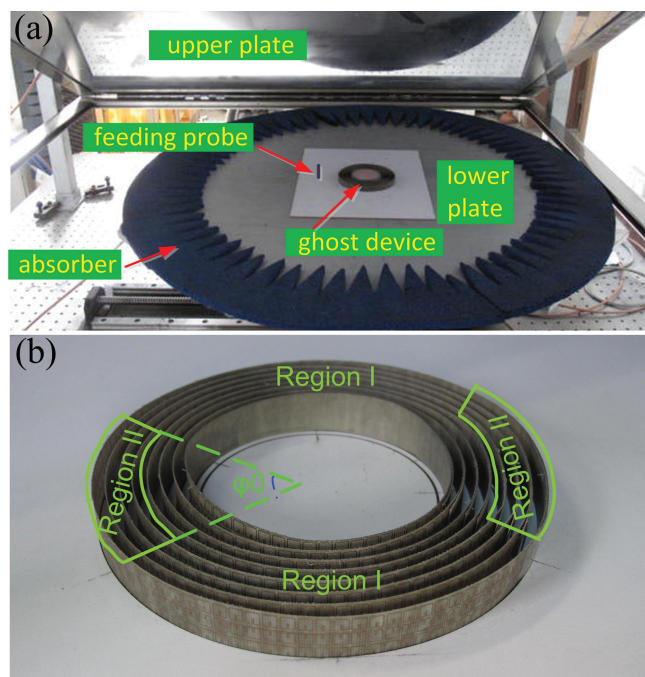


Figure 6. a) The photograph of the parallel-plate waveguide mapping system. b) The photograph of the fabricated ghost-illusion device.

electric-field distributions (see Figure 6a). The electric fields were polarized in the vertical direction confined by two large aluminum plates, whose distance is set as 12 mm. The electric field was detected and scanned by a monopole probe embedded in the top aluminum plate. The feeding and detection probes were connected to two ports of network analyzer via thin coaxial cables. The ghost-device sample was fixed on the center of the bottom plate, which was mounted on a computer-controlled stage that can move in two dimensions. The scanning region covered $4.27\lambda_0 \times 4.67\lambda_0$ ($128 \times 140 \text{ mm}^2$) with a step resolution of 1 mm.

Fabricated Ghost Device and Experiment Platform: The photograph of a fabricated ghost device is shown in Figure 6b. The detailed values of geometry and material parameters are illustrated in Table 1. Throughout the paper, $\phi_0 = 60^\circ$.

Table 1. The geometrical parameters h_1 and h_2 of the ghost device, and the associated values of ϵ_z and μ_r . The imaginary parts of the electro-magnetic parameters are small enough to be neglected.

Number of Layers	Region I			Region II		
	h_1 [mm]	ϵ_z	μ_r	h_2 [mm]	ϵ_z	μ_r
1	0.894	2.847	0.086			
2	0.939	2.835	0.127			
3	0.986	2.824	0.168			
4	1.057	2.810	0.218			
5	1.097	2.803	0.244	0.618	6.253	0.244
6	1.162	2.793	0.279	0.776	6.229	0.279
7	1.228	2.785	0.311	0.957	6.207	0.311
8	1.298	2.776	0.341	1.169	6.185	0.341

Acknowledgements

W.X.J. and C.W.Q. contributed equally to this work. This work was supported in part from the National Science Foundation of China under Grant Nos. 60990320, 60990321, 60990324, 61171024, 61171026, 60910111, and 60921063, in part from the National High Tech (863) Projects under Grant Nos. 2011AA010202 and 2012AA030402, in part from the 111 Project under Grant No. 111-2-05, in part from the Fundamental Research Funds for the Central Universities, and in part by the Joint Research Center on Terahertz Science. C. W. Q. acknowledges the Mindef-NUS JPP Grant of R-263-000-A38-232 and R-263-000-A38-133, administrated by National University of Singapore.

Received: December 21, 2012

Revised: January 17, 2013

Published online: March 12, 2013

- [1] U. Leonhardt, T. Philbin, *Geometry and Light: The Science of Invisibility*, Dover, Downers Grove 2010.
- [2] *Metamaterials—Theory, Design, and Applications*, (Ed: T. J. Cui, D. R. Smith, R. Liu), Springer, New York 2009.
- [3] J. B. Pendry, D. Schurig, D. R. Smith, *Science* **2006**, 312, 1780.
- [4] J. B. Pendry, A. Aubry, D. R. Smith, S. A. Maier, *Science* **2012**, 337, 549.
- [5] U. Leonhardt, *Science* **2006**, 312, 1777.
- [6] S. Zhang, D. A. Genov, C. Sun, X. Zhang, *Phys. Rev. Lett.* **2008**, 100, 123002.
- [7] D. Gevaux, *Nat. Phys.* **2009**, 5, 16.
- [8] J. Li, J. B. Pendry, *Phys. Rev. Lett.* **2008**, 101, 203901.
- [9] R. Liu, C. Ji, J. J. Mock, J. Y. Chin, T. J. Cui, D. R. Smith, *Science* **2009**, 323, 366.
- [10] J. Valentine, J. Li, T. Zentgraf, G. Bartal, X. Zhang, *Nat. Mater.* **2009**, 8, 568.
- [11] L. H. Gabrielli, J. Cardenas, C. B. Poitras, M. Lipson, *Nat. Photonics* **2009**, 3, 461.
- [12] X. Chen, Y. Luo, J. Zhang, K. Jiang, J. B. Pendry, S. Zhang, *Nat. Commun.* **2011**, 2, 176.
- [13] B. Zhang, Y. Luo, X. Liu, G. Barbastathis, *Phys. Rev. Lett.* **2011**, 106, 033901.
- [14] H. F. Ma, T. J. Cui, *Nat. Commun.* **2010**, 1, 21.
- [15] Y. Lai, H. Y. Chen, D. Z. Han, J. J. Xiao, Z.-Q. Zhang, C. T. Chan, *Phys. Rev. Lett.* **2009**, 102, 253902.
- [16] W. X. Jiang, H. F. Ma, Q. Cheng, T. J. Cui, *Appl. Phys. Lett.* **2010**, 96, 121910.
- [17] C. Li, X. K. Meng, X. Liu, F. Li, G. Y. Fang, H. Y. Chen, C. T. Chan, *Phys. Rev. Lett.* **2010**, 105, 233906.
- [18] W. X. Jiang, T. J. Cui, *Phys. Rev. E* **2011**, 83, 026601.
- [19] W. X. Jiang, T. J. Cui, H. F. Ma, X. M. Yang, Q. Cheng, *Appl. Phys. Lett.* **2011**, 98, 204101.
- [20] Y. G. Ma, C. K. Ong, T. Tyc, U. Leonhardt, *Nat. Mater.* **2009**, 8, 639.
- [21] N. Kundtz, D. R. Smith, *Nat. Mater.* **2009**, 9, 129.
- [22] H. F. Ma, T. J. Cui, *Nat. Commun.* **2010**, 1, 124.
- [23] T. C. Han, C.-W. Qiu, X. H. Tang, *Opt. Lett.* **2010**, 35, 2642.
- [24] Y. Lai, H. Chen, Z.-Q. Zhang, C. T. Chan, *Phys. Rev. Lett.* **2009**, 102, 093901.
- [25] D. Liang, J. Gu, J. Han, Y. Yang, S. Zhang, W. Zhang, *Adv. Mater.* **2012**, 24, 916.
- [26] Y. Yang, A. Q. Liu, L. K. Chin, X. M. Zhang, D. P. Tsai, C. L. Lin, C. Lu, G. P. Wang, N. I. Zheludev, *Nat. Commun.* **2012**, 3, 651.
- [27] Y. Yang, L. K. Chin, J. M. Tsai, D. P. Tsai, N. I. Zheludev, A. Q. Liu, *Lab Chip* **2012**, 12, 3785.
- [28] H. Chen, C. T. Chan, P. Sheng, *Nat. Mater.* **2010**, 9, 387.
- [29] H. Chen, X. Zhang, X. Luo, H. Ma, C. T. Chan, *New J. Phys.* **2008**, 10, 113016.